Supporting Information for:

Insights into the Interaction between Immobilized Biocatalysts and Metal-Organic Frameworks: A Case Study of PCN-333

Wenjie Yang,[†§], Weibin Liang,[†*], Luke A. O'Dell,[‡] Hamish D. Toop,[‖] Natasha Maddigan,[‖] Xingmo Zhang,[†] Alena Kochubei,[§] Christian J. Doonan,[‖] Yijiao Jiang,[§] Jun Huang[†*]

[†] Laboratory for Catalysis Engineering, School of Chemical and Biomolecular Engineering, Sydney Nano Institute, the University of Sydney, NSW 2006, Australia

[§] Department of Engineering, Macquarie University, Sydney, NSW 2019, Australia

[‡] Institute for Frontier Materials, Deakin University, Geelong, VIC 3220, Australia

[‖] Department of Chemistry and the Centre for Advanced Nanomaterials, The University of Adelaide, Adelaide, South Australia 5005, Australia

*Email: weibin.liang@sydney.edu.au, jun.huang@sydney.edu.au

Table of Contents

Content		Page
S1	77K N_2 sorption isotherms of PCN-333 and enzyme@PCN-333 biocomposites	S2
S2	Bradford assay for enzyme loading	S3
S3	Attenuated total reflection Fourier transform infrared spectroscopy (ATR-FTIR)	S4
S4	Scanning electron microscopy (SEM)	S5
S5	Confocal Laser Scanning Microscopy (CLSM)	S6
S6	Catalytic test of supernatant of FITC-Lipase@PCN-333	S7
S7	Inductively Coupled Plasma Mass Spectrometer (ICP-MS)	S8
S8	Solid-state NMR measurements	S9
S9	Synthesis, characterization, and enzymatic activity of HRP@PCN-333	S15
S10	References	S19

S1 77K N_2 sorption isotherms of PCN-333 and enzyme@PCN-333 biocomposites

The textural properties of PCN-333 and enzyme@PCN-333 is evaluated by N_2 sorption isotherms. Based on the results demonstrated in Figure S1, the BET surface areas is calculated to be 4198, 172, and 130 m^2 g^{-1} for PCN-333, Lipase@PCN-333, and Insulin@PCN-333, respectively. The much smaller specific surface areas of enzyme@PCN-333 compared with PCN-333 indicates the successful immobilization of guest enzymes into the pores of PCN-333 host.

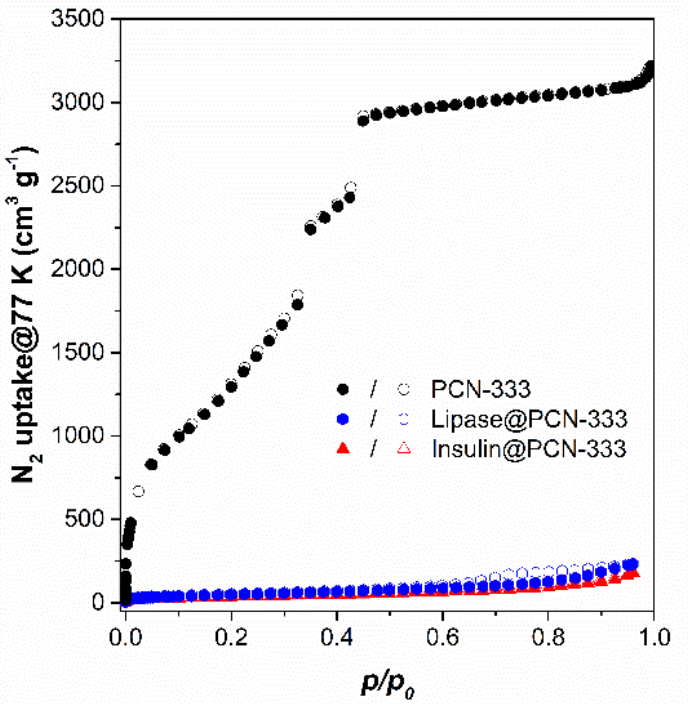

Figure S1 77K N_2 sorption isotherms of PCN-333 (black), Lipase@PCN-333 (blue), and Insulin@PCN-333 (red). The filled and open symbols in Figure S1 represents the adsorption and desorption isotherms, respectively.

S2 Bradford assay for enzyme loading

To quantitatively measure the loading amount of enzymes in enzyme@PCN-333, the dye-binding assays, Bradford assay is conducted, which determined the concentration of biomolecule in the supernatant (Figure S2). To calculate the quantities of immobilized biomolecule in enzyme@PCN-333, the quantity difference between the amounts of biomolecule used in the synthesis and those in the collected supernatant is calculated. Figure S2 demonstrates that the loading of lipase and insulin in Lipase@PCN-333 and Insulin@PCN-333 are 26.9 and 50.0 mg g^{-1}, respectively.

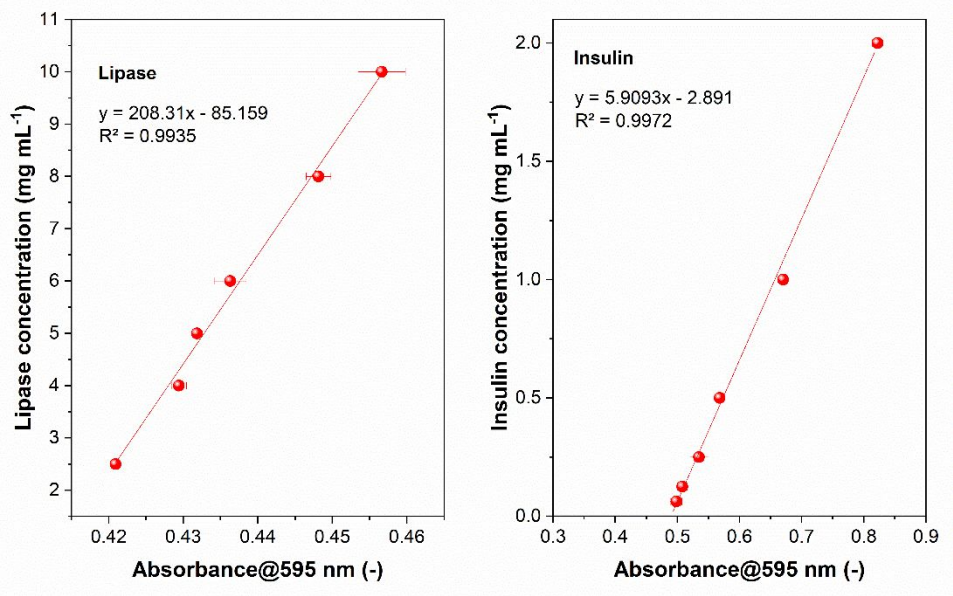

Figure S2 The calibration curves of lipase (a) and insulin (b using the Bradford assay. Error bars are generated from triplicate experiments.

S3 Attenuated total reflection Fourier transform infrared spectroscopy (ATR-FTIR)

The ATR-FTIR measurements were conducted on a Thermo Nicolet iS50 infrared spectrometer.

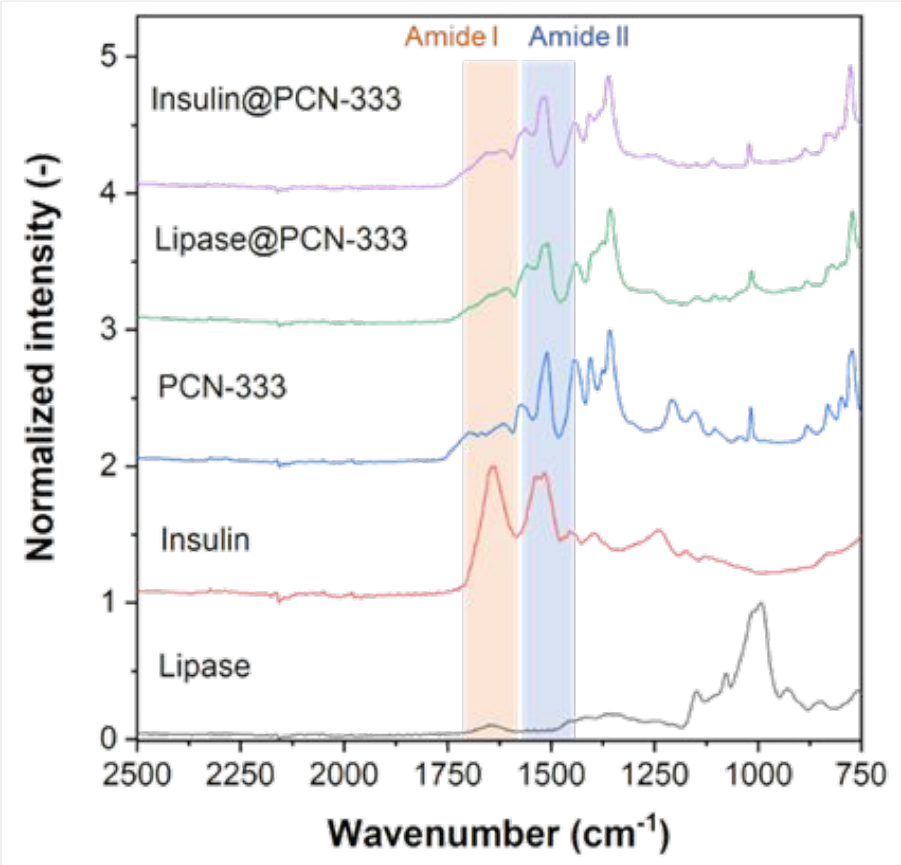

Figure S3 ATR-FTIR spectra (2500−750 cm^{-1}) of lipase (grey), insulin (red), PCN-333 (blue), Lipase@PCN-333 (green), and Insulin@PCN-333 (purple). The characteristic region of amide I (1700-1610 cm^{-1}) and amide II (1595-1480 cm^{-1}) in the peptide backbone are highlighted in orange and blue boxes, respectively.[1-2]

S4 Scanning electron microscopy (SEM)

SEM images were collected using a Zeiss ULTRA Plus Scanning Electron Microscope. Prior to analysis, the samples were dispersed in ethanol by sonication, drop-cast on an aluminum SEM stage (12 mm), and sputter-coated with gold to form a thin film (5 nm).

The morphologies of PCN-333 and enzyme@PCN-333 is observed by scanning electron microscopy. Demonstrated by SEM images (Figure S4), PCN-333, Lipase@PCN-333, and Insulin@PCN-333 samples have bulk structure of octahedral crystals, and the size of which is ca. 300 nm. Additionally, after the immobilization of enzymes, one can identify that the structure of octahedral crystals of enzyme@PCN-333 is less well defined.

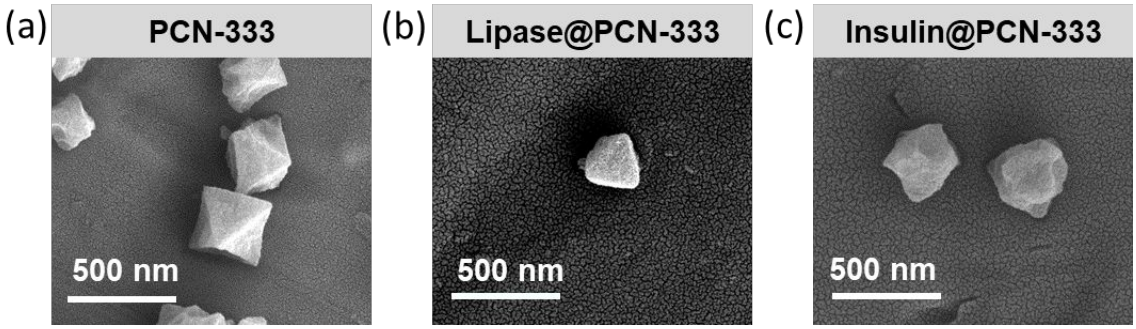

Figure S4 SEM images for PCN-333 (a), Lipase@PCN-333 (b), and Insulin@PCN-333 (c)

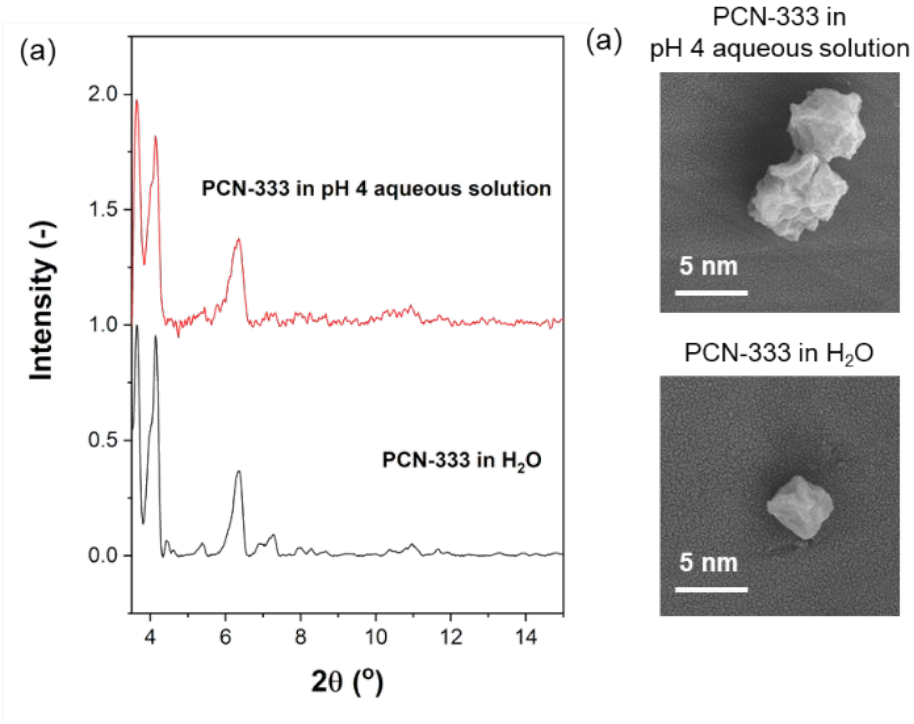

Figure S5 PXRD patterns (a) and SEM images (b) of PCN-333 soaked in H_2O or diluted HCl aqueous solution (pH 4, 20 mM) for 1h.

S5 Confocal Laser Scanning Microscopy (CLSM)

The presence and spatial localization of the fluorophore-tagged lipase in PCN-333 was determined by CLSM (Olympus FV3000 Confocal Laser Scanning Microscope). The FITC-tagged lipase was excited at 488 nm and the fluorescence signal was collected from 495 – 545 nm.

The FITC-lipase@PCN-333 biocomposite visualized via confocal laser scanning micrographs (Figure S6) further confirms the presence of lipase enzyme in/on the FITC-lipase@PCN-333 biocomposite.

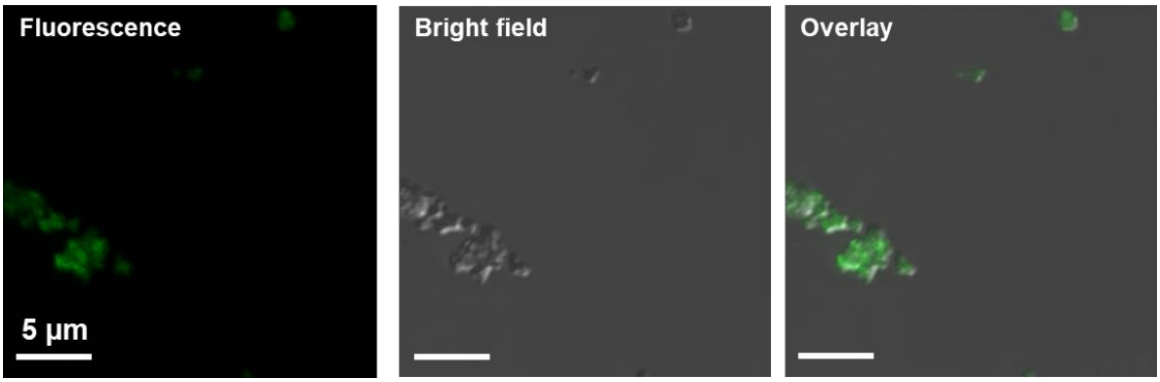

Figure S6 Confocal laser scanning micrographs showing fluorescence (left), bright field (middle), and overlay (right) images of FITC-lipase@PCN-333 biocomposite. The scale bars for all images are 5 µm.

S6 Catalytic test of supernatant of FITC-Lipase@PCN-333

Experiments to determine the potential FITC-lipase leaching from FITC-lipase@PCN-333 were carried out as per the catalytic activity of FITC-lipase@PCN-333. Catalytic assays were measured after a reaction time of 2 min.

A suspension of FITC-lipase@PCN-333 in deionised water (50 µL) was incubated in an aqueous solution of Tris buffer (940 µL, 50 mM, pH 7.4) under static condition at room temperature for 20 h. Thereafter, the mixture was centrifuged (13.5k RPM, 30 sec) and the supernatant collected. The catalytic assay was started with the addition of 4-nitrophenyl butyrate, and the activity measured. Positive control experiments were completed either directly as included in the main text or, to determine whether the FITC-lipase was stable in Tris buffer. FITC-lipase in deionised water (5 µL, 5 mg mL^{-1}) was added to a solution of aqueous Tris buffer solution (985 µL, 50 mM, pH 7.4). The solution was left to stand at room temperature for 20 h before the reaction was started with the addition of 4-nitrophenyl butyrate and the activity measured.

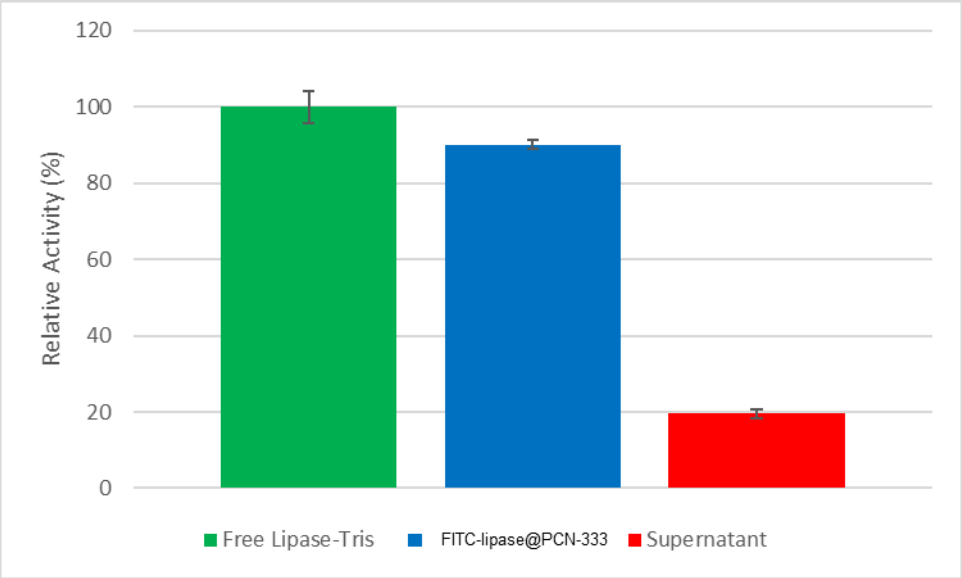

Figure S7 Comparison of the relative catalytic activity of FITC-lipase@PCN-333, free FITC-lipase, and a supernatant collected after incubating FITC-lipase@PCN-333 in Tris buffer for 20 h. Experiments were performed in triplicate with standard error shown for each run.

After being incubated in Tris-buffer overnight, the FITC-lipase@PCN-333 shows an approximately 15% activity loss. In addition, the collected supernatant from the incubation solution of FITC-lipase@PCN-333 shows an around 20% relative activity. The ICP-MS results (Table S1 and S2) corroborate well with the activity results shown in Figure S7. In the supernatant solution, no aluminum (from PCN-333 framework) was detected (Table S1). However, a significant amount of sulfur was measured in the supernatant (Table S2), when compared to the Tris-buffer solution control. The sulfur in the supernatant is contributed by the amino acids in lipase containing sulfur, such as cysteine and methionine.

S7 Inductively Coupled Plasma Mass Spectrometer (ICP-MS)

ICP-MS was performed on an Agilent 8900x QQQ-ICP-MS. The amount of PCN-333 in solution was calculated according to a standard calibration curve for aluminium, prepared from a standard solution from High Purity Standards (10 mg L^{-1} Al in 2% aq. HNO_3, HPS-Q17617A). The amount of protein in solution was calculated according to a standard calibration curve for sulfur, prepared from a standard solution from High Purity Standards (10 mg L^{-1} S in 2% aq. HNO_3, Cat#: 10 54-5).

The FITC-lipase@PCN-333 was removed from the catalytic reaction solution by centrifugation. Supernatant from a FITC-lipase@PCN-333 sample was collected. Thereafter, 5 µL of the supernatant solution was added to an aqueous solution of nitric acid (286 µL, 35 %, Seastar Chemicals, S010101-CHEQ09). The solution was left to stand at room temperature for 48 h. Thereafter, the samples were diluted to a total volume of 5 mL with Milli-Q water for ICP-MS analysis. A control of the Tris buffer was made by adding Tris buffer (5 µL, 50 mM, pH 7.4) to a solution of aqueous nitric acid (286 µL, 35 %, Seastar Chemicals, S010101-CHEQ09). The solution was left to stand at room temperature for 48 h. then, diluted to a total volume of 5 mL with Milli-Q water for ICP-MS analysis.

Table S1 ICP-MS results comparing the aluminium content (in ppb) of the Tris buffer and a supernatant collected after incubating FITC-lipase@PCN-333 in Tris buffer for 20 h. Experiments were performed in triplicate.

	Conc. (ppb)	St. Dev.	N
Tris Buffer Control 1	12.391	0.636	3
Tris Buffer Control 1	7.448	0.370	3
Tris Buffer Control 1	1.914	0.196	3
	7.251	4.555	
Lip@PCN-333 SN 1	2.423	0.168	3
Lip@PCN-333 SN 2	2.374	0.311	3
Lip@PCN-333 SN 3	3.388	0.203	3
	2.728	0.536	

Table S2 ICP-MS results comparing the sulfur content (in ppb) of the Tris buffer and a supernatant collected after incubating FITC-lipase@PCN-333 in Tris buffer for 20 h. Experiments were performed in triplicate.

	Conc. (ppb)	St. Dev.	N
Tris Buffer Control 1	14.362	3.827	3
Tris Buffer Control 1	< 4.566	0	3
Tris Buffer Control 1	< 4.566	1.557	3
	7.832	5.316	
Lip@PCN-333 SN 1	29.329	1.150	3
Lip@PCN-333 SN 2	44.642	2.496	3
Lip@PCN-333 SN 3	31.258	1.122	3
	35.076	7.374	

S8 Solid-state NMR measurements

S8.1 Relaxation spectroscopy

For ^{1}H spin-lattice relaxation analysis, as the magnetization of ^{1}H nuclei can rapidly diffuse throughout the entire spin network of the solid, a relatively uniform T_1 value for all protons in the domain is expected. Due to the strong homonuclear dipolar-dipolar interactions, the high natural abundance of the ^{1}H nuclei, and the fast magic-angle spinning rate (12 KHz), the ^{1}H T_1 value of a specific position can be utilized to represent the molecular dynamics of the entire network.

Inset in Figure S8a gives ^{1}H T_1 values for different proton species in PCN-333 and enzyme@PCN-333. In the inversion recovery pulses ^{1}H spectrum of PCN-333, the T_1 values across the whole set of ^{1}H peaks were calculated. Inset in Figure 8b gives ^{27}Al T_1 values for different proton species in PCN-333 and enzyme@PCN-333. As the relaxation times for the ^{27}Al nuclei are much shorter than those of the ^{1}H nuclei, instead of applying inversion recovery pulses, saturation recovery pulses were utilized to measure the recovery speed of the net magnetization of ^{27}Al nuclei. The ^{27}Al T_1 values for the same peak (Al^{VI} species) of all different samples are calculated and the relaxation curve is shown in Figure S8b.

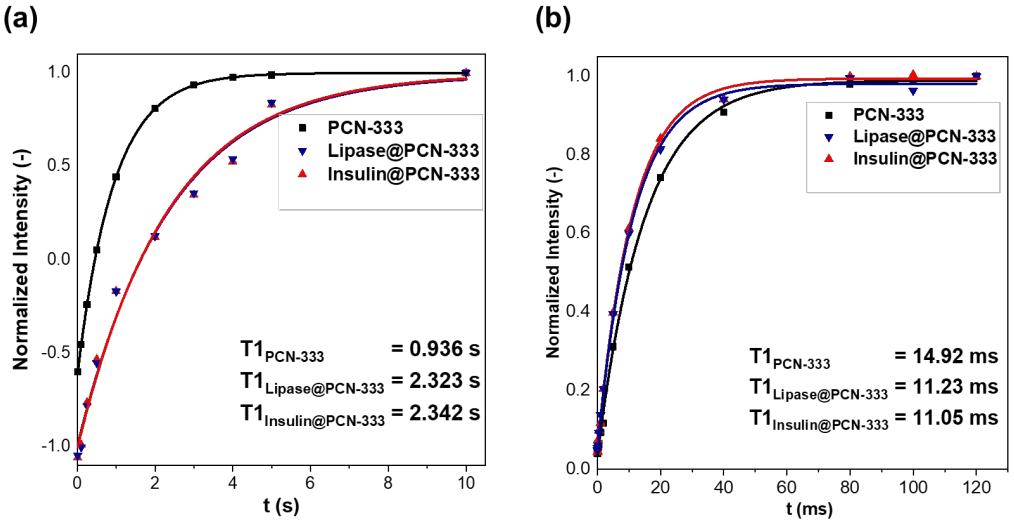

Figure S8 Molecular dynamics measurements for PCN-333 (in black line and square symbol), Lipase@PCN-333 (in blue line and triangle symbol), and Insulin@PCN-333 (in red line and triangle symbol) via relaxation spectroscopy. (a)^{1}H ssNMR T_1 spin-lattice relaxation measurements; (b) ^{27}Al ssNMR T_1 spin-lattice relaxation measurements

S8.2 ^{13}C Cross-polarization MASNMR spectroscopy

To separate C1 and C6 species of PCN-333 in the ^{13}C spectra (Figure 4a), spectra deconvolution is conducted using DMFit.[3] Since ^{13}C is a half-spin nucleus with I = ½, Gaussian line shape is applied to establish a faithful deconvolution. Based on the deconvolution result, after the enzyme immobilization, the C1 species showed no change while a high-field shift is observed for C6 species (Figure 4b and Table S3).

Table S3 Summary of ^{13}C CP MASNMR spectra deconvolution results

	δ^{13}C		
	C1 species (ppm)	C6 species (ppm)	DMF (ppm)
PCN-333	173	171	165
Insulin@PCN-333	173	169	-
Lipase@PCN-333	173	169	165

S8.3 ^{1}H single-pulse ssNMR spectroscopy for enzymes

To confirm the proton assignment of enzyme@PCN-333 in the ^{1}H spectra (Figure 4a), The ^{1}H MAS NMR measurements for free Insulin and Lipase were conducted. The spectra for free enzymes are similar and revealed mainly the signals from aliphatic proton (~0-4 ppm), water and NH_2 functionalities (~4.8-5.2 ppm)[4-5].

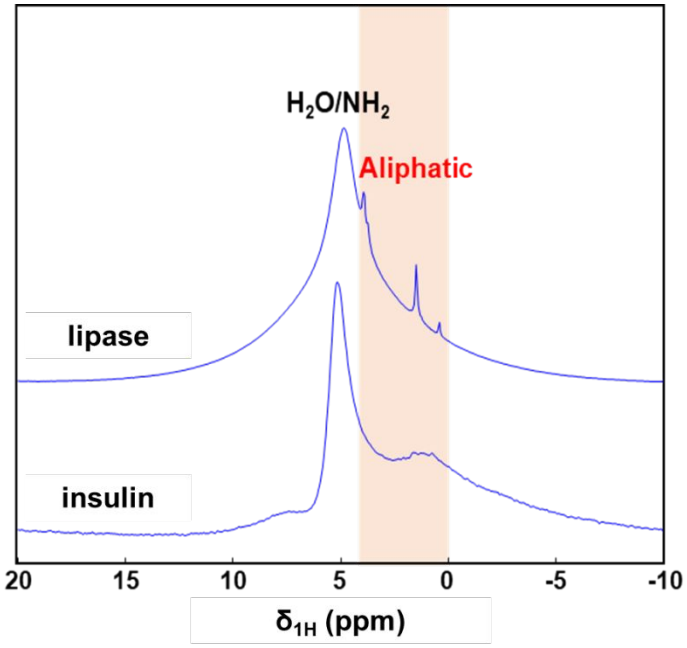

Figure S9 The ^{1}H MAS NMR spectra of insulin and lipase.

S8.4 ^{27}Al single-pulse NMR spectroscopy

The single pulse ^{27}Al ssNMR was applied to visualize the local coordination of Al-oxo cluster in PCN-333 and enzyme@PCN-333. The solely peak in the spectra (0-15 ppm) suggested that all aluminum atoms in the host are Al^{VI} species.

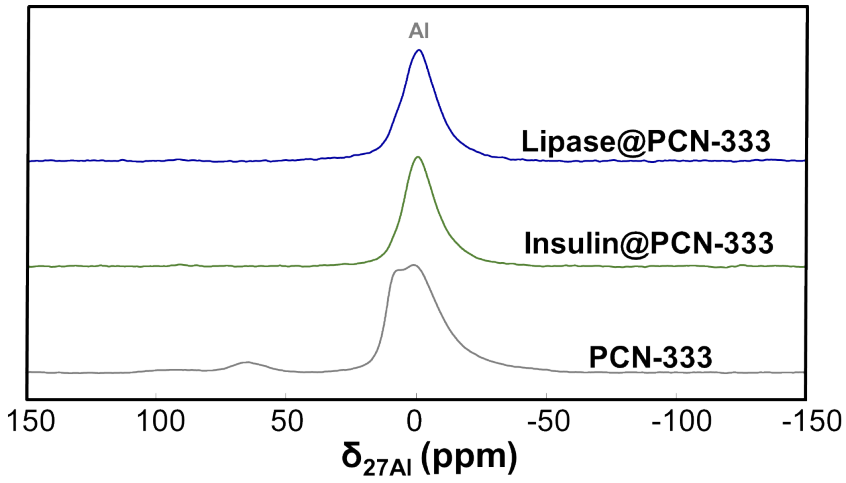

Figure S10 The ^{27}Al single-pulse ssNMR spectra of enzyme@PCN-333 samples.

Since ^{27}Al is a quadrupolar nucleus, the second order quadrupolar interaction resulted anisotropic line shape in the MAS NMR spectra makes the deconvolution via Gaussian/Lorentzian line fitting unreliable. While the difference of the global shape of ^{27}Al spectra can indicate the change of the chemical environment of the Al centers in PCN-333 after enzyme immobilization.

Table S4 Summary of line width (full width at half maximum, FWHM) of Al^{VI} peaks in the ^{27}Al MASNMR spectra

	FWHM of Al^{VI} peak (Hz)
PCN-333	2901
Insulin@PCN-333	1754
Lipase@PCN-333	1956

S8.5 ^{27}Al Multi-quantum MASNMR spectroscopy

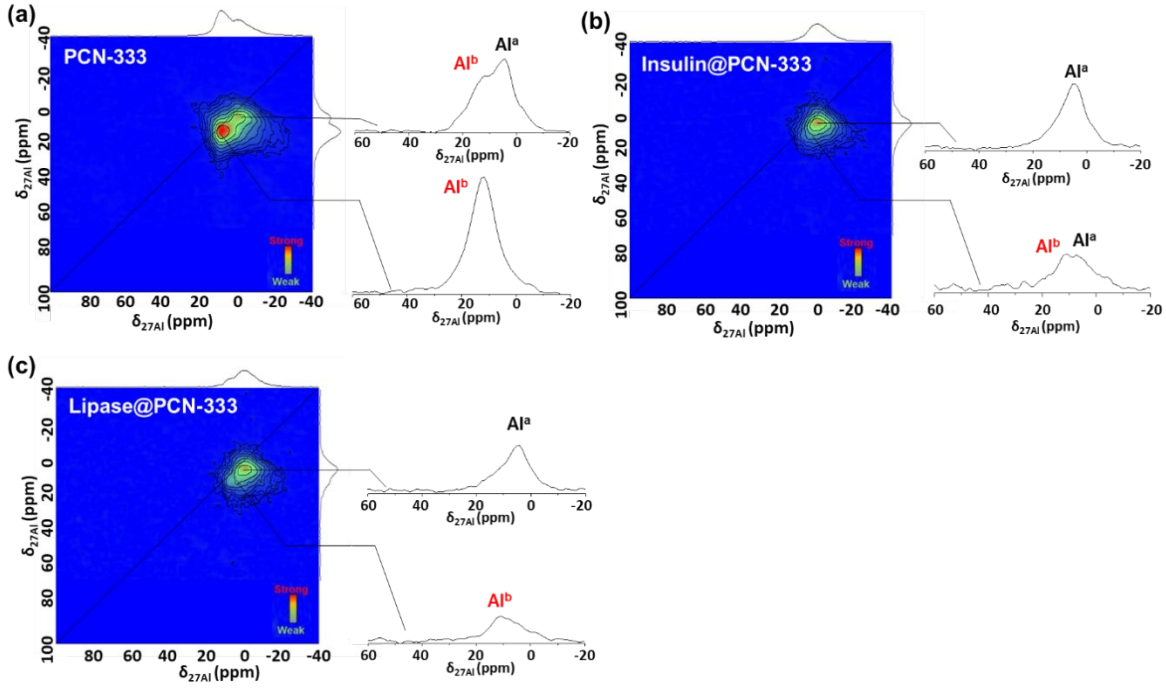

Figure S11 PCN-333 aluminum site local structure investigation. 2D ^{27}Al MQMAS NMR spectra and corresponding slides of (a) PCN-333, (b) Insulin@PCN-333, (c) Lipase@PCN-333.

Based on ^{27}Al MQ MAS NMR spectra, quadrupolar tensors have been defined in DMFit.[3] The quadrupolar parameters for each subspecies can be obtained via the identification of contour in the 2D MQ ^{27}Al MAS NMR (Figure S11) and the application of equation 1-4 (See experimental for details). Isotropic chemical shift (δ_{iso}) represents the position of the specific subspecies in the corresponding 1D MAS NMR spectrum, and the quadrupolar coupling constant (C_{QCC}) indicates the degree of distortion of the specific subspecies. The larger C_{QCC} of a species, the less isotropic of its local environment.[6]

Table S5 Summary of 2D MQ ^{27}Al MAS NMR quadrupolar parameters*.

	δ_{iso}[a] (ppm)	C_{QCC}[b] (MHz)
PCN-333-Al^a	2.7	2.15
PCN-333-Al^b	10.0	1.93
Insulin@PCN-333-Al^a	2.5	2.24
Insulin@PCN-333-Al^b	10.4	2.01
Lipase@PCN-333-Al^a	2.6	2.17
Lipase@PCN-333-Al^b	10.7	2.25

* quadrupolar parameters are calculated via applying equation 1-4 (See experimental for details)

[a] Isotropic chemical shift (δ_{iso})

[b] quadrupolar coupling constant (C_{QCC}) of each aluminum species.

S8.6 $^{1}H/^{27}Al$ TRAPDOR NMR spectroscopy

The $^{1}H/^{27}Al$ TRAPDOR NMR spectroscopy was measured to understand the spatial relationship between Al-oxo cluster of PCN-333 host and specific protons from either host or guest. As an NMR technique, the TRAPDOR sequence can be utilized to ascertain spatial information such as proximity, connectivity, and interaction via facilitating the recoupling of the heteronuclear dipole coupling between ^{27}Al quadrupole and ^{1}H nuclei[7]. Without REDOR pulse, all proton signals can be observed in the ^{1}H spectra; while after the application of 50W ^{27}Al dephasing pulse with 160 μs irradiation period, the adjacent ^{1}H-^{27}Al pair dephasing, which suppress the peak intensity of the specific proton. Thus, via the subtraction of the 50W ^{27}Al dephasing pulse ^{1}H spectrum from ^{1}H spectrum obtained without REDOR pulse, the information regarding the ^{1}H and ^{27}Al with proximity can be obtained[8-9].

As shown in Figure S12, after the immobilization of enzymes, a small difference observed between S and S_0 spectra indicates the spatial proximity between the Al-oxo clusters and the -NH_2 groups. Note that the flexibility of PCN-333 MOF structure gives difficulty in the formation of strong and stable dipolar coupling which could suppress the ^{1}H and ^{27}Al pair dephasing[10], thereby only tiny peaks can be observed in the TRAPDOR difference spectra.

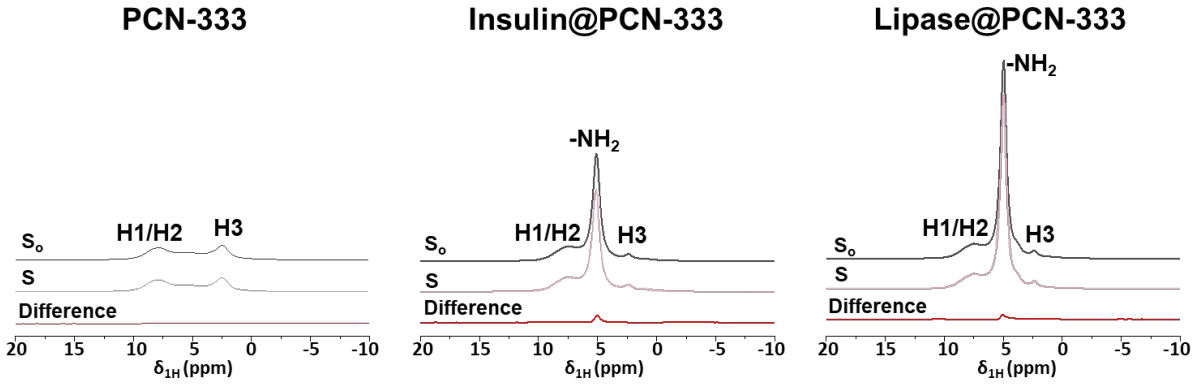

Figure S12 The $^{1}H/^{27}Al$ TRAPDOR NMR spectra of enzyme@PCN-333 samples. S_0 (Black lines): spectra obtained without REDOR pulse; S (Pink lines): spectra obtained with 50W ^{27}Al dephasing pulse. Difference (red lines): difference spectra = S_0-S.

S9 Synthesis, characterization, and enzymatic activity of HRP@PCN-333

S9.1 Synthesis and characterization of HRP@PCN-333

Due to the limitation of CLSM, we failed to distinguish the surface-absorbed FITC-lipase biomolecules from the infiltrated ones in FITC-lipase@PCN-333. Proteolytic enzymes, such as trypsin and protease, are often used to digest enzymes absorbed on the surface of the MOF biocomposites.[11] In principle, the MOF can act as a size-selective coating to prevent the ingress of trypsin molecules into its pores and protect the infiltrated/encapsulated enzymes. Trypsin treatment has been applied in the literature to demonstrate the advantage of MOF protection as well as to qualitatively evidence the success of enzyme infiltration (and/or encapsulation) by comparing the bioactivity of the enzyme@MOF biocomposites before and after trypsin treatment.[11-13] However, in our case, the p-nitrophenyl ester also acts as a substrate for proteolytic enzymes, such as trypsin.[14] Because of the possible interference of residue trypsin on the enzymatic assay test, enzymatic test after trypsin treatment is not an ideal strategy to deactivate the surface-absorbed FITC-lipase on FITC-lipase@PCN-333 and to confirm the success of FITC-lipase infiltration in FITC-lipase@PCN-333.

To elucidate whether the immobilized proteins are encapsulated within the pores of PCN-333, HRP@PCN-333 (HRP = horseradish peroxidase; Sigma-Aldrich, lyophilized, powder, ~150 U mg^{-1}) were synthesized and tested for its enzymatic activity before and after trypsin treatment. Trypsin is a proteolytic agent[15] which can hydrolyze the surface-adsorbed HRP on PCN-333 and deactivate their enzymatic activity. If the HRP biomolecules are only surface-absorbed on the PCN-333 crystallites, a progressive loss of activity will be observed. However, if the HRP biomolecules are infiltrated/encapsulated in the mesopores of PCN-333, a plateau of the bioactivity of HRP/PCN-333 will be observed after trypsin treatment, indicating the success of infiltration/encapsulation. In the enzymatic assay test, ABTS (2,2'-azino-bis(3-ethylbenzothiazoline-6-sulfonate) was used as a chromogen for the hydrogen peroxide assay of HRP.[16]

The synthesis and wash procedure of HRP@PCN-333 was analogous to that of Lipase@PCN-333 (see Experimental for details). After synthesis, HRP@PCN-333 was subjected to PXRD analysis to determine the crystallinity of the material. As indicated in Figure S13, PCN-333 retained its crystallinity after HRP immobilization.

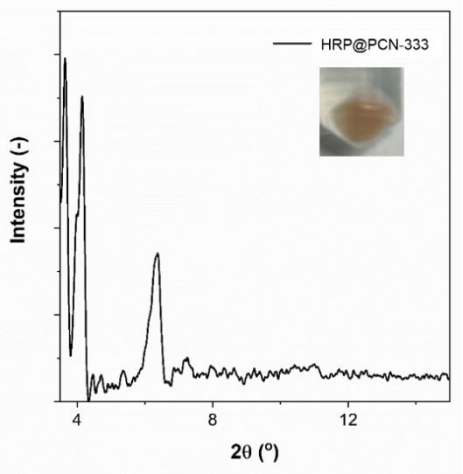

Figure S13 Experimental PXRD pattern of HRP@PCN-333. The digital image of HRP@PCN-333 was shown as inset of the figure.

The success of HRP immobilization in/on PCN-333 was first indicated by the reddish color of the resulting materials (inset in Figure S13). To determine the immobilization efficiency of the HRP in/on PCN-333, a calibration curve for HPR was measured by

using Bradford assay (Figure S14). Accordingly, the HRP loading in HRP@PCN-333 was calculated to be 20.1 mg g^{-1} with a loading efficiency of 40.2%.

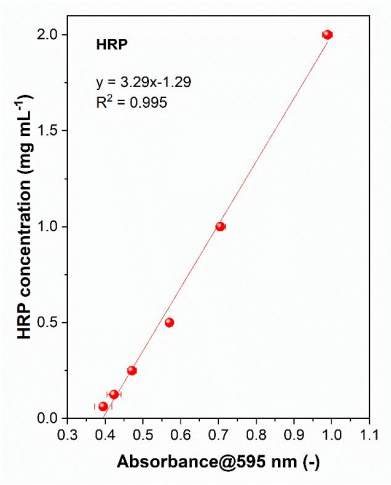

Figure S14 The calibration curves of HRP using the Bradford assay. Error bars are generated from triplicate experiments.

The porosity of HRP@PCN-333, 77 K N_2 sorption experiment was conducted, and the result is shown in Figure S15. Similar to Lipase@PCN-333 and Insulin@PCN-333, the BET surface area of HRP@PCN-333 drop significantly as compared to the pristine PCN-333 sample. The pore size distribution of HRP@PCN-333 was further calculated based on the 77 K N_2 adsorption isotherm and presented in Figure S15. Besides the micropore centered at 1.1 nm, one mesoporous cavity centered at ~4.0 nm was detected for HRP@PCN-333 sample (Figure S15). The disappearance of the largest mesopore (ø = 5.5 nm, HRP (4.0 x 4.4 x 6.8 nm, Figure S16)) in HRP@PCN-333 points to the successful HRP encapsulation in HRP@PCN-333.

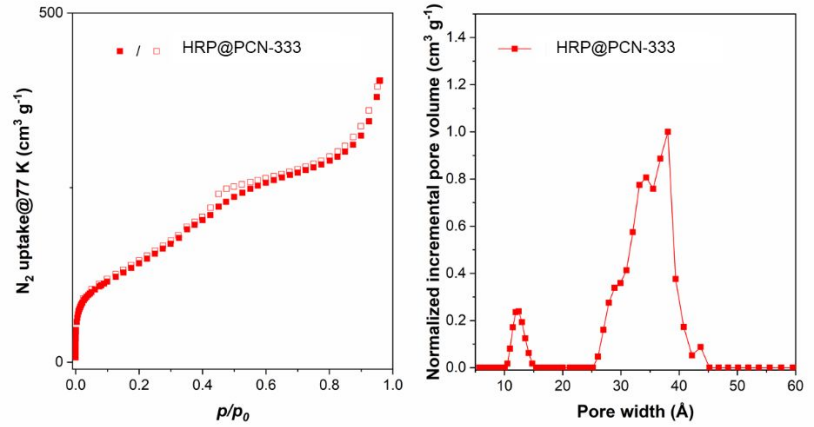

Figure S15 77K N_2 sorption isotherms of HRP@PCN-333 (left). The filled and open symbols represent the adsorption and desorption isotherms, respectively. Pore size distribution (right) of HRP@PCN-333 was calculated using NLDFT model based on the N_2 adsorption isotherms measured at 77 K.

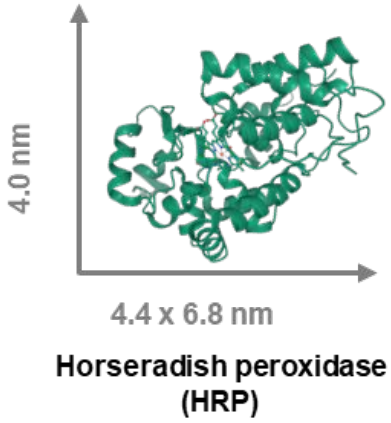

Figure S16 Molecular structure of HRP (PDB 1W4Y).

S9.2 Enzymatic assay analysis

In the next step, we sought to examine and compare the bioactivity of free HRP and HRP@PCN-333. Prior to the HRP and HRP@PCN-333 test, control experiments confirms that trypsin do not catalyze the ABTS assay (Figure S17a). In a typical enzymatic assay experiment, 2.5 mL of ABTS (ABTS-RO, ABTS™ Tablets, Sigma Aldrich) solution (0.5 mg mL^{-1} in 0.1 M pH 7.4 aqueous Tris-HCl buffer solution), 0.05 mL of HRP stock solution (0.1 mg mL^{-1} in 0.1 M pH 7.4 aqueous Tris-HCl buffer solution) and 0.05 mL Tris-HCl buffer solution (0.1 M, pH 7.4) was mixed in a quartz cuvette. Thereafter, 0.1 mL of diluted H_2O_2 (30% (w/w) in H_2O, Sigma Adrich) solution (88.2 mM) was introduced. The color evolution of the assay was monitored the A_{405nm} by using a UV-vis spectrophotometer (Shimadzu UV-3600i Plus). The trypsin (Trypsin from porcine pancreas, lyophilized powder, Type II-S, 1000-2000 units/mg dry solid, Sigma Aldrich) treatment was carried out as follow: after mixing the HRP stock solution with trypsin stock solution (10 mg mL^{-1} in 0.1 M pH 7.4 aqueous Tris-HCl buffer solution) in an Eppendorf centrifuge tube (2 mL), the mixture was stored at room temperature for 6 h prior to enzymatic assay test.

As shown in Figure S17a, HRP@PCN-333 shows an 85.0% enzymatic activity of HRP as compared to the free HRP, which may be caused by the diffusion control of the bulky ABTS substrate. After trypsin treatment, only 26.7% of the original bioactivity was retained for free HRP, while 93.1% in the case of HRP@PCN-333 (Figure S17b). These results confirm that the HRP biomolecules are actually infiltrated/encapsulated inside the pores of PCN-333 and the PCN-333 can act as a protective layer for the infiltrated HRP, preventing the ingress of trypsin. Similar results are reported for HRP@ZIF-8.[11] It is worth to noting that the HRP@ZIF-8 was washed with surfactant to remove any surface bound proteins and ascertain the success of HRP encapsulation. The success of HRP encapsulation in ZIF-8 were also demonstrated by comparing the bioactivity of HRP@ZIF-8 biocomposite before and after trypsin treatment. After trypsin treatment, HRP@ZIF-8 biocomposite retained the bioactivity of HRP showing an 88% conversion of pyrogallol to purpurogallin. In comparison, only 20% conversion was observed for an analogous experiment for free HRP after trypsin treatment.[11] In another example, CAT@ZIF-90 retained 91.8% of its original enzymatic activity after proteinase K treatment, while free catalase completely lost its bioactivity under analogous treatment.[12]

In combination of the PXRD, sorption analysis, CLSM and enzymatic activity test (Figure 1, S6, and S13-17), as well as by comparing our experimental results with literature examples, we qualitatively conclude that the immobilized enzyme molecules are successfully infiltrated/encapsulated into the pore of enzyme@PCN-333.

Due to the interference of paramagnetic iron-heme in HRP for the ssNMR measurement, HRP@PCN-333 was not subjected for ssNMR test.

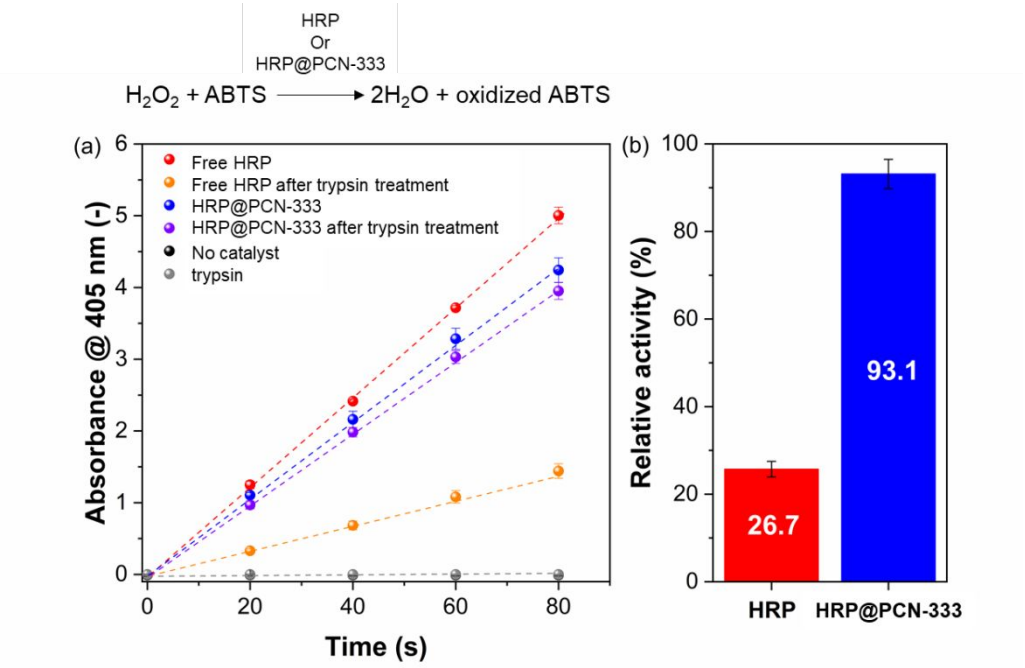

Figure S17 (a) Catalytic activity of free HRP (red), HRP@PCN-333 (blue), free HRP after trypsin treatment (orange), and HRP@PCN-333 after trypsin treatment (purple). The assay was performed in Tris-HCl buffer (pH 7.4, 0.1 M) with 5 μg of catalyst (based on the weight of HRP). The H_2O_2 concentration was 3.2 mM. The ABTS concentration was 0.46 mg mL^{-1}. Error bars are generated from triplicate experiments. (b) Retained bioactivity (in relative activity (%) as compared to the original bioactivity of the materials without trypsin treatment) of HRP (red) and HRP@PCN-333 (blue) after trypsin treatment.

S10 References

1. Barth, A., Infrared spectroscopy of proteins. *Biochimica et Biophysica Acta (BBA) - Bioenergetics* **2007,** *1767*, 1073-1101.
2. Jackson, M.; Mantsch, H. H., The Use and Misuse of FTIR Spectroscopy in the Determination of Protein Structure. *Critical Reviews in Biochemistry and Molecular Biology* **1995,** *30*, 95-120.
3. Massiot, D.; Fayon, F.; Capron, M.; King, I.; Le Calvé, S.; Alonso, B.; Durand, J. O.; Bujoli, B.; Gan, Z.; Hoatson, G., Modelling one-and two-dimensional solid-state NMR spectra. *Magn. Reson. Chem.* **2002,** *40*, 70-76.
4. Jiang, Y.; Huang, J.; Marx, S.; Kleist, W.; Hunger, M.; Baiker, A., Effect of dehydration on the local structure of framework aluminum atoms in mixed linker MIL-53 (Al) materials studied by solid-state NMR spectroscopy. *J. Phys. Chem. Lett.* **2010,** *1*, 2886-2890.
5. Varghese, S.; Halling, P. J.; Häussinger, D.; Wimperis, S., High-resolution structural characterization of a heterogeneous biocatalyst using solid-state NMR. *J. Phys. Chem. C* **2016,** *120*, 28717-28726.
6. Xu, J.; Wang, Q.; Li, S.; Deng, F., *Solid-state NMR in zeolite catalysis*. Springer: 2019; Vol. 103.
7. Grey, C. P.; Vega, A. J., Determination of the quadrupole coupling constant of the invisible aluminum spins in zeolite HY with 1H/27Al TRAPDOR NMR. *J. Am. Chem. Soc.* **1995,** *117*, 8232-8242.
8. Zeng, Q.; Nekvasil, H.; Grey, C. P., Proton environments in hydrous aluminosilicate glasses: a 1H MAS, 1H/27Al, and 1H/23Na TRAPDOR NMR study. *J. Phys. Chem. B* **1999,** *103*, 7406-7415.
9. Wang, Z.; Buechel, R.; Jiang, Y.; Wang, L.; Xu, H.; Castignolles, P.; Gaborieau, M.; Lafon, O.; Amoureux, J.-P.; Hunger, M., Engineering the Distinct Structure Interface of Subnano-alumina Domains on Silica for Acidic Amorphous Silica–Alumina toward Biorefining. *JACS Au* **2021**.
10. Wang, Z.; Jiang, Y.; Jin, F.; Stampfl, C.; Hunger, M.; Baiker, A.; Huang, J., Strongly enhanced acidity and activity of amorphous silica–alumina by formation of pentacoordinated AlV species. *J. Catal.* **2019,** *372*, 1-7.
11. Liang, K.; Ricco, R.; Doherty, C. M.; Styles, M. J.; Bell, S.; Kirby, N.; Mudie, S.; Haylock, D.; Hill, A. J.; Doonan, C. J.; Falcaro, P., Biomimetic mineralization of metal-organic frameworks as protective coatings for biomacromolecules. *Nat. Commun.* **2015,** *6*, 7240.
12. Shieh, F.-K.; Wang, S.-C.; Yen, C.-I.; Wu, C.-C.; Dutta, S.; Chou, L.-Y.; Morabito, J. V.; Hu, P.; Hsu, M.-H.; Wu, K. C. W.; Tsung, C.-K., Imparting Functionality to Biocatalysts via Embedding Enzymes into Nanoporous Materials by a de Novo Approach: Size-Selective Sheltering of Catalase in Metal–Organic Framework Microcrystals. *J. Am. Chem. Soc.* **2015,** *137*, 4276-4279.
13. Liang, W.; Xu, H.; Carraro, F.; Maddigan, N. K.; Li, Q.; Bell, S. G.; Huang, D. M.; Tarzia, A.; Solomon, M. B.; Amenitsch, H., Enhanced activity of enzymes encapsulated in hydrophilic metal–organic frameworks. *J. Am. Chem. Soc.* **2019,** *141*, 2348-2355.
14. Stewart, J. A.; Ouellet, L., The trypsin-catalyzed hydrolysis of p-nitrophenyl acetate. *Can. J. Chem.* **1959,** *37*, 751-9.
15. Rawlings, N. D.; Salvesen, G.; Editors, *Handbook of Proteolytic Enzymes, 3rd Edition*. Academic Press: 2012; p 4094 pp.
16. Bergmeyer, H. U.; Editor, *Methods of Enzymatic Analysis, Vol. 9: Proteins and Peptides. 3rd Ed*. VCH: 1986; p 571 pp.